ANTIMICROBIAL AGENTS AND CHEMOTHERAPY, Dec. 2002, p. 3802–3808 Vol. 46, No. 12
0066-4804/02/$04.00+0 DOI: 10.1128/AAC.46.12.3802–3808.2002

Effect of Auristatin PHE on Microtubule Integrity and Nuclear Localization in *Cryptococcus neoformans*

Tanja Woyke,[1,2] Robert W. Roberson,[3] George R. Pettit,[1,4] Günther Winkelmann,[2] and Robin K. Pettit[1,5]*

Cancer Research Institute,[1] and Departments of Microbiology,[5] and Chemistry and Biochemistry,[4] and Department of Plant Biology, Molecular and Cellular Biology Program,[3] Arizona State University, Tempe, Arizona 85287, and Eberhard Karls University Tübingen, 72076 Tübingen, Germany[2]

Received 20 March 2002/Returned for modification 12 June 2002/Accepted 19 August 2002

The mechanism of action of the fungicidal peptide auristatin PHE was investigated in *Cryptococcus neoformans*. Since auristatin PHE causes budding arrest in *C. neoformans* (T. Woyke, G. R. Pettit, G. Winkelmann, and R. K. Pettit, Antimicrob. Agents Chemother. 45:3580-3584, 2001), microtubule integrity and nuclear localization in auristatin PHE-treated cells were examined. Iterative deconvolution in conjunction with an optimized *C. neoformans* microtubule immunolabeling procedure enabled detailed visualization of the microtubule cytoskeleton in auristatin PHE-treated *C. neoformans*. The effect of auristatin PHE on *C. neoformans* microtubule organization was compared with that of the tubulin-binding agent nocodazole. Both drugs produced complete disruption first of cytoplasmic and then of spindle microtubules in a time- and concentration-dependent manner. Sub-MICs of auristatin PHE caused complete microtubule disruption within 4.5 h, while 1.5 times the nocodazole MIC was required for the same effect. For both drugs, disruption of microtubules was accompanied by blockage of nuclear migration and of nuclear and cellular division, resulting in cells arrested in a uninucleate, large-budded stage. Nocodazole and the linear peptide auristatin PHE are remarkably different in structure and spectrum of activity, yet on the cellular level, they have similar effects.

The basidiomycetous budding yeast *Cryptococcus neoformans* was identified as a human pathogen more than 100 years ago (5). Due to the growing number of immunocompromised patients worldwide, the number of invasive infections caused by this encapsulated yeast has been increasing dramatically (6, 15, 29, 42). The most frequent clinical manifestation of cryptococcal infection is meningoencephalitis, which is fatal if left untreated. Existing therapies, including polyene and azole antifungals (11, 29, 42, 49), are limited by host toxicities (42) and the emergence of drug-resistant strains (18, 20).

The pentapeptide auristatin PHE (dovaline-valine-dolaisoleunine-dolaproine-phenylalanine-methyl-ester) is a synthetic modification of the natural marine product dolastatin 10 (37, 38), which is currently undergoing phase I and phase II cancer clinical trials. Auristatin PHE has fungicidal activity against *C. neoformans* and fungicidal or fungistatic activity against various species of *Trichosporon* (39, 50). Auristatin PHE caused *C. neoformans* cells to arrest in a large-budded stage (50), suggesting that it might interfere with the microtubule dynamics in a manner similar to that of nocodazole in *Saccharomyces cerevisiae* (17).

To investigate this possibility, we optimized cell wall digestion and microtubule labeling conditions for *C. neoformans*. This procedure, in conjunction with iterative deconvolution microscopy, allowed detailed visualization of the *C. neoformans* microtubule network. In iterative deconvolution, the focal Z plane sections are digitally captured and out-of-focus light in each section is mathematically removed and/or reduced by examination of neighboring sections (2, 43). This leads to image contrast and resolution that are far superior to those achieved with either standard epifluorescence microscopy or laser scanning confocal microscopy (3, 28). With these techniques, the microtubule networks of control, auristatin PHE-treated, and nocodazole-treated *C. neoformans* were compared.

MATERIALS AND METHODS

Yeast strain and growth conditions. *C. neoformans* 90112 was obtained from the American Type Culture Collection (Manassas, Va.). The strain was maintained on yeast morphology (YM) agar (Difco Laboratories, Detroit, Mich.). Cultures for microscopy were grown in YM broth (Difco Laboratories) at 35°C and incubated with rotary shaking at 280 rpm.

Antifungal agents. Auristatin PHE (M_r =760) was synthesized and purified using standard purification procedures as previously described (37, 38). Aliquots were stored desiccated in the dark at room temperature. Prior to each experiment, auristatin PHE was reconstituted in dimethyl sulfoxide (DMSO) to a concentration of 200 μg/0.1 ml. Stock solutions of 100 μg of nocodazole [methyl-5-(2-thienylcarbonyl)-1-*H*-benzimidazole-2-yl-carbamate] (Sigma Chemical Co., St. Louis, Mo.)/ml were prepared in DMSO and stored as frozen aliquots at −20°C. Auristatin PHE and nocodazole were diluted in YM broth to the appropriate concentrations, while the concentration of DMSO was maintained at 0.8%.

Drug treatments. MICs for *C. neoformans* 90112 were determined by broth microdilution according to the NCCLS standard (33). The MIC of auristatin PHE was 0.5 μg/ml in RPMI 1640 medium and 4 μg/ml in YM broth, and the nocodazole MIC was 0.03 μg/ml in RPMI medium and 0.06 μg/ml in YM broth. For immunofluorescent staining of microtubules, early-logarithmic-phase cultures of *C. neoformans* in YM broth were treated with 0.7 to 15.8 μM auristatin PHE or 0.03 to 0.6 μM nocodazole for 0.5 to 4.5 h in a rotary shaker at 35°C and 280 rpm. These concentrations represent 0.125 to 3 times the MIC of the corresponding compound as determined by broth microdilution in YM broth. For nuclear localization analysis, a 3.5-h exposure to 0.03 to 8 times the MIC (0.2 to 42.1 μM auristatin PHE; 0.006 to 1.6 μM nocodazole) of each compound was used. For microtubule staining and nuclear localization experiments, DMSO

* Corresponding author. Mailing address: Cancer Research Institute, Arizona State University, Tempe, AZ 85287-2404. Phone: (480) 965-4907. Fax: (480) 965-8558. E-mail: pettitr@asu.edu.

controls and drug-treated samples contained 0.8% DMSO. Cells were prepared for microscopy immediately after each treatment period.

Immunofluorescent staining. Cultures of *C. neoformans* ($\sim 2 \times 10^6$ cells/ml) were fixed according to the method of Pringle et al. (40). Briefly, 8% aqueous formaldehyde (Electron Microscopy Sciences, Fort Washington, Pa.) was added directly to the culture to a final concentration of 4%. After 10 min, cells were postfixed in phosphate-buffered formaldehyde (50 mM potassium phosphate, 0.5 mM $MgCl_2$, 4% formaldehyde) and incubated for an additional 2 h. For immunolabeling of the microtubule cytoskeleton, fixed cells were rinsed twice in phosphate sorbitol buffer (PSB, comprising 1 M sorbitol and 0.1 M potassium phosphate [pH 7.0]). This buffer enhanced labeling and preserved microtubules better than phosphate-buffered saline (PBS, comprising 0.1 M phosphate buffer and 0.15 M NaCl [pH 6.8]) or piperazine-*N*,*N*′-bis(2-ethanesulfonic acid) (PIPES) buffer. Cell wall digestion was attempted with glusulase and zymolyase according to the work of Pringle et al. (40) and with Novozym 234 (Calbiochem-Novabiochem Corp., La Jolla, Calif.) at 0.1 to 2% with digestion times of 1 to 60 min. Various combinations of different detergents, protease inhibitors, and sulfhydryl reducing agents were evaluated, and incubation with antibodies was assessed at 4°C, room temperature, and 35°C. Microtubules were most efficiently stained as follows. The cell wall was partially digested with 1% Novozym in PSB containing 0.1% bovine serum albumin (BSA), 0.25 μl of β-mercaptoethanol/ml, 50 μg of phenylmethylsulfonyl fluoride/ml, and 5 μg of aprotinin/ml (Sigma) for 45 min. Cells were rinsed first in PSB and then in PBS and were subsequently treated for 10 min with 0.1% Nonidet P-40 in PBS containing 4 mM $MgCl_2$ and 4 mM EGTA. Cells were rinsed in PBS and incubated with an anti-α-tubulin monoclonal antibody (immunoglobulin G; Accurate Chemical and Scientific Corporation, Westbury, N.Y.) diluted 500-fold in PBS–0.1% BSA–0.01% sodium azide (PBS-BSA) for 12 to 24 h. After a rinse in PBS, cells were incubated for 12 to 24 h in the dark with a goat anti-mouse antibody conjugated to Alexa 488 (A-11017; Molecular Probes, Eugene, Oreg.) diluted 100-fold in PBS-BSA, and nuclei were stained with 0.1 μg of 4′,6-diamidino-2-phenylindole (DAPI; Sigma)/ml in H_2O for 5 min. All labeling steps were performed in Eppendorf tubes at room temperature. Labeled cells were allowed to settle on acid-washed, poly-L-lysine (Sigma)-coated coverslips and were mounted on glass slides in 90% glycerol–10% 0.1 M PBS (pH 8.6)–2% *n*-propyl gallate (Sigma).

Visualization of bud scars and nuclei. For visualization of bud scars, formaldehyde-fixed cells were stained with 10 μg of wheat germ agglutinin conjugated with tetramethyl rhodamine isocyanate (TRITC; Sigma)/ml for 10 min at room temperature. To visualize nuclei, cells were washed in PBS and stained with DAPI as described above. Stained cells were mounted as described above.

Image capture and analysis. Tubulin-labeled cells were examined using an Eclipse TE300 inverted microscope (Nikon, Garden City, N.Y.) equipped for differential interference contrast optics and epifluorescent viewing with a 150-W xenon bulb and appropriate filters. All images were observed with a Plan-Neofluor 100×/1.4 (oil immersion) objective, captured using a low-light-level Quantix charge-coupled device camera (Roper Scientific Inc., Tucson, Ariz.), and processed with Isee software (Inovision Corp., Raleigh, N.C.). Thirty optical sections were captured at 0.2-μm intervals, and out-of-focus light was removed by iterative deconvolution. Untreated cells were selected and arranged in a temporal sequence based on the developmental characteristics of the microtubules. For microtubule imaging in drug-treated *C. neoformans* over time, image capturing was performed at drug concentrations equivalent to 1.5 times the MIC (as determined in YM broth) for both auristatin PHE (7.9 μM) and nocodazole (0.3 μM). Deconvolved image projections were collapsed into two dimensions. Images were processed in Photoshop 6.0 (Adobe Systems, Mountain View, Calif.) and printed using an NP-1600 M Medical Color Printer (Codonics, Inc., Middleburg Heights, Ohio). Three independent experiments were performed. At each given time point and drug concentration, ≥200 cells were examined. Images were described as follows: control-like, if >90% of the stained cells had an intact microtubule network; disrupted with spindles present, if >90% of the stained cells had disrupted microtubules but spindles were present; completely disrupted, if >90% of the stained cells had completely disrupted cytoplasmic and spindle microtubules; completely disrupted with accumulation of tubulin fragments in two distinct areas of the cell, if >90% of the cells fit this description.

To determine the location and number of nuclei in drug-treated versus control cells, a minimum of 200 budding, wheat germ agglutinin-TRITC- and DAPI-stained cells were counted and described for each of three independent experiments, and standard errors of the means were calculated. Cells were examined using an Eclipse TE300 inverted microscope equipped with appropriate filters. Images were captured at drug concentrations equivalent to 1.5 times the MIC (as determined in YM broth) for both auristatin PHE (7.9 μM) and nocodazole (0.3 μM). Images were processed and printed as described above.

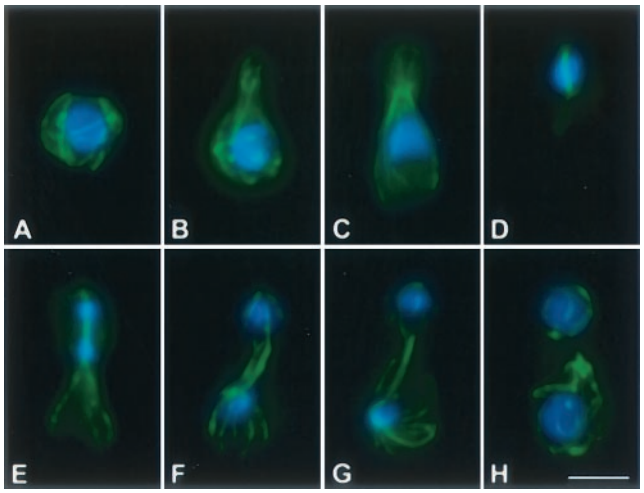

FIG. 1. Microtubule cytoskeleton and nuclear position during the *C. neoformans* cell cycle. Immunofluorescent imaging of microtubules (anti-α-tubulin antibodies) was merged with nuclear staining (DAPI). Individual cells are arranged in their presumed order during the cell cycle (from panel A to panel H). Bar, 5 μm.

RESULTS

Optimized microtubule visualization. Many variables in fixation, cell wall digestion, and immunostaining were compared to optimize microtubule preservation and labeling in *C. neoformans*. Methods described for microtubule staining of other yeasts (40) served as a starting point. The optimized procedure included postfix washing in PSB containing 1 M sorbitol; partial cell wall digestion with 1% Novozym 234, β-mercaptoethanol, and protease inhibitors; and plasma membrane extraction with Nonidet P-40. Furthermore, deconvolution yielded images superior to those obtained by confocal microscopy or standard epifluorescence microscopy.

Drug-induced disruption of microtubules. The microtubule cytoskeleton of *C. neoformans* exhibited distinct developmental patterns throughout the vegetative cell cycle. Abundant interphase cytoplasmic microtubules, mostly localized subcortically, formed a loosely interwoven meshwork surrounding the nucleus (Fig. 1A). Microtubules extended into the bud, parallel to its growing axis, as the bud emerged (Fig. 1B). During mitosis, cytoplasmic microtubules became less abundant, while spindle and astral microtubules assembled (Fig. 1C and D). Astral microtubules were abundant and appeared to associate with the cell cortex (Fig. 1E, F, and G). Upon the completion of mitosis, cytoplasmic microtubules reappeared as spindle and astral microtubules depolymerized (Fig. 1H). Cytoplasmic interphase microtubules extended longitudinally as well as tangentially throughout the cytoplasm, surrounding the nucleus (Fig. 1A, B, and H).

Immunofluorescent tubulin staining of auristatin PHE- and nocodazole-treated *C. neoformans* revealed that both compounds caused disruption of microtubules in a concentration- and time-dependent manner. At 0.5 times the MIC (2.6 μM), auristatin PHE caused complete microtubule disruption within 4.5 h (Table 1). Nocodazole caused complete disruption between 2.5 and 3.5 h at 1.5 times the MIC (0.3 μM) (Table 1). Exposure to 7.9 μM auristatin PHE (1.5 times the MIC) re-

TABLE 1. Degree of microtubule disruption during treatment with various concentrations of auristatin PHE and nocodazole

Concn[a]	Result[b] at the following exposure time (h):					
	0	0.5	1.5	2.5	3.5	4.5
Auristatin PHE						
0.7 (0.1)	○	○	○	○	○	○
2.6 (0.5)	○	○	○	●	●	●●
5.3 (1)	○	○	●	●	●	●●●
7.9 (1.5)	○	●	●	●●	●●●	●●●
10.5 (2)	○	●	●●	●●	●●●	●●●
15.8 (3)	○	●	●●	●●	●●●	●●●
Nocodazole						
0.03 (0.1)	○	○	○	○	○	○
0.1 (0.5)	○	○	○	○	○	○
0.2 (1)	○	○	○	○	○	●
0.3 (1.5)	○	○	●	●	●●●	●●●
0.4 (2)	○	○	●	●●	●●●	●●●
0.6 (3)	○	●	●●	●●	●●●	●●●

[a] Expressed as a micromolar concentration and (in parentheses) as the concentration relative to the MIC. For example, 0.7 μM auristatin PHE is equivalent to 0.1 times the MIC.

[b] Symbols: ○, DMSO control-like; ●, disrupted microtubules, with spindles present; ●●, completely disrupted cytoplasmic and spindle microtubules; ●●●, complete disruption and accumulation of tubulin fragments in two distinct areas of the cell.

sulted in a slow and gradual disappearance of the microtubule cytoskeleton (Table 1; Fig. 2), with initial disruption of microtubules occurring by 30 min (Table 1; Fig. 2B). Increased disruption occurred after 1.5 h, and by 2.5 h tubulin-associated fluorescence was restricted to five to eight bright plaques distributed throughout the mother cell and bud cytoplasm (Table 1; Fig. 2D). During late stages of treatment with either drug, tubulin-associated fluorescence was primarily limited to two bright plaques, one located in the mother cell and one in the bud (Table 1; Fig. 2E). Nocodazole exposure took slightly longer to achieve the same degree of microtubule-inhibitory effects, but once disruption started, the microtubule cytoskeleton disappeared within approximately 1 h (Table 1; Fig. 3). In the presence of either drug, spindle microtubules were more stable than cytoplasmic microtubules (see, e.g., Fig. 2C). DMSO alone had no noticeable effect on the *C. neoformans* microtubule cytoskeleton (data not shown). Rhodamine-phalloidin staining revealed that neither auristatin PHE nor nocodazole visibly affected the actin cytoskeleton of *C. neoformans* at drug concentrations up to 3 times the MIC (15.8 μM auristatin PHE; 0.6 μM nocodazole) (data not shown).

The MIC of auristatin PHE (as determined in RPMI medium) for *S. cerevisiae* is >64 μg/ml (50)). At concentrations up to 263.2 μM (200 μg/ml) and exposure times up to 12 h, auristatin PHE had no apparent effect on the *S. cerevisiae* microtubule network (data not shown).

Drug-induced blockage of nuclear migration and cytoplasmic and nuclear division. Since microtubules are essential for nuclear migration and division in budding yeasts (16, 17), we examined nuclear localization in drug-treated *C. neoformans*. Wheat germ agglutinin-TRITC was used to reveal bud scars on previously divided *C. neoformans* mother cells. A 3.5-h exposure to various concentrations (sub-MIC to 8 times the MIC) of auristatin PHE or nocodazole demonstrated a concentration-dependent increase in mother cells containing a single nucleus, while binuclear arrangements with one nucleus in the mother cell and one nucleus in the daughter cell decreased (Fig. 4). This inhibition of nuclear migration and division started to occur at sub-MICs and plateaued at 3 times the MIC for both drugs; at this concentration, approximately 90% of the cell population was uninucleate, with the nucleus in the mother cell (Fig. 4). Within the auristatin PHE-treated cell population, approximately 3% of the cells had two nuclei in the mother cell at drug concentrations of 0.5 and 1 times the MIC (Fig. 4A). Figure 5 shows representative images of control cells (Fig. 5A) and cells treated with 1.5 times the MIC of auristatin PHE (Fig. 5B) or nocodazole (Fig. 5C).

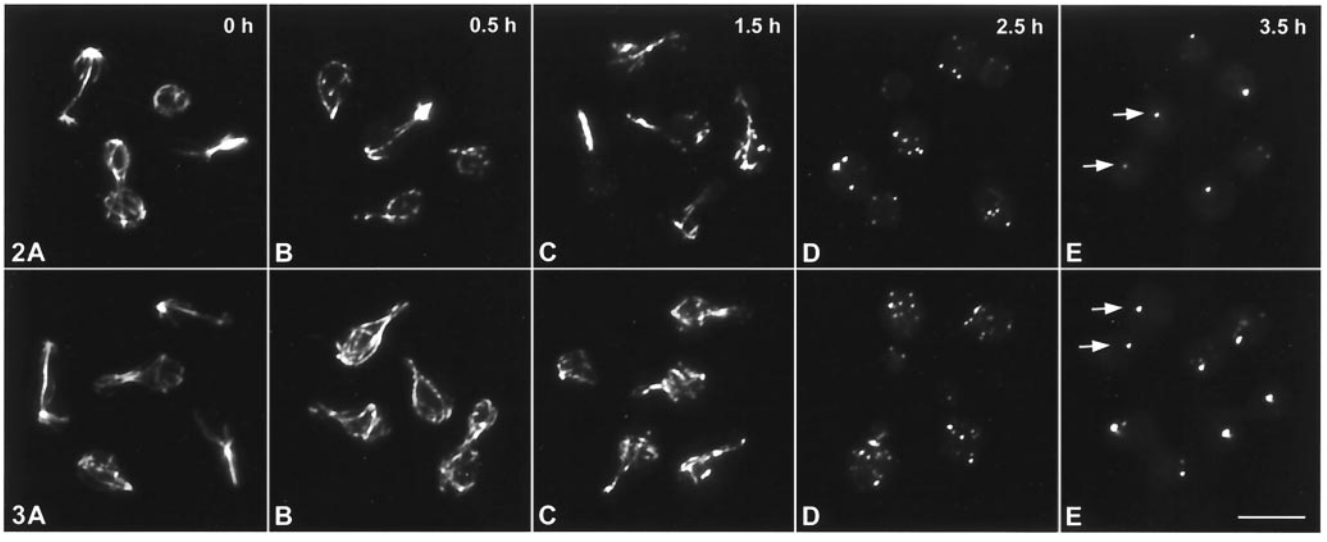

FIG. 2 and 3. Immunofluorescent imaging of microtubule disruption in drug-treated *C. neoformans* cells. Cells were fixed 0 (A), 0.5 (B), 1.5 (C), 2.5 (D), and 3.5 (E) h after treatment with 7.9 μM auristatin PHE (1.5 times the MIC) (Fig. 2) or 0.3 μM nocodazole (1.5 times the MIC) (Fig. 3). After 3.5 h, tubulin remnants accumulated in two discrete regions in the mother cell and the daughter cell (arrows). Bar, 5 μm.

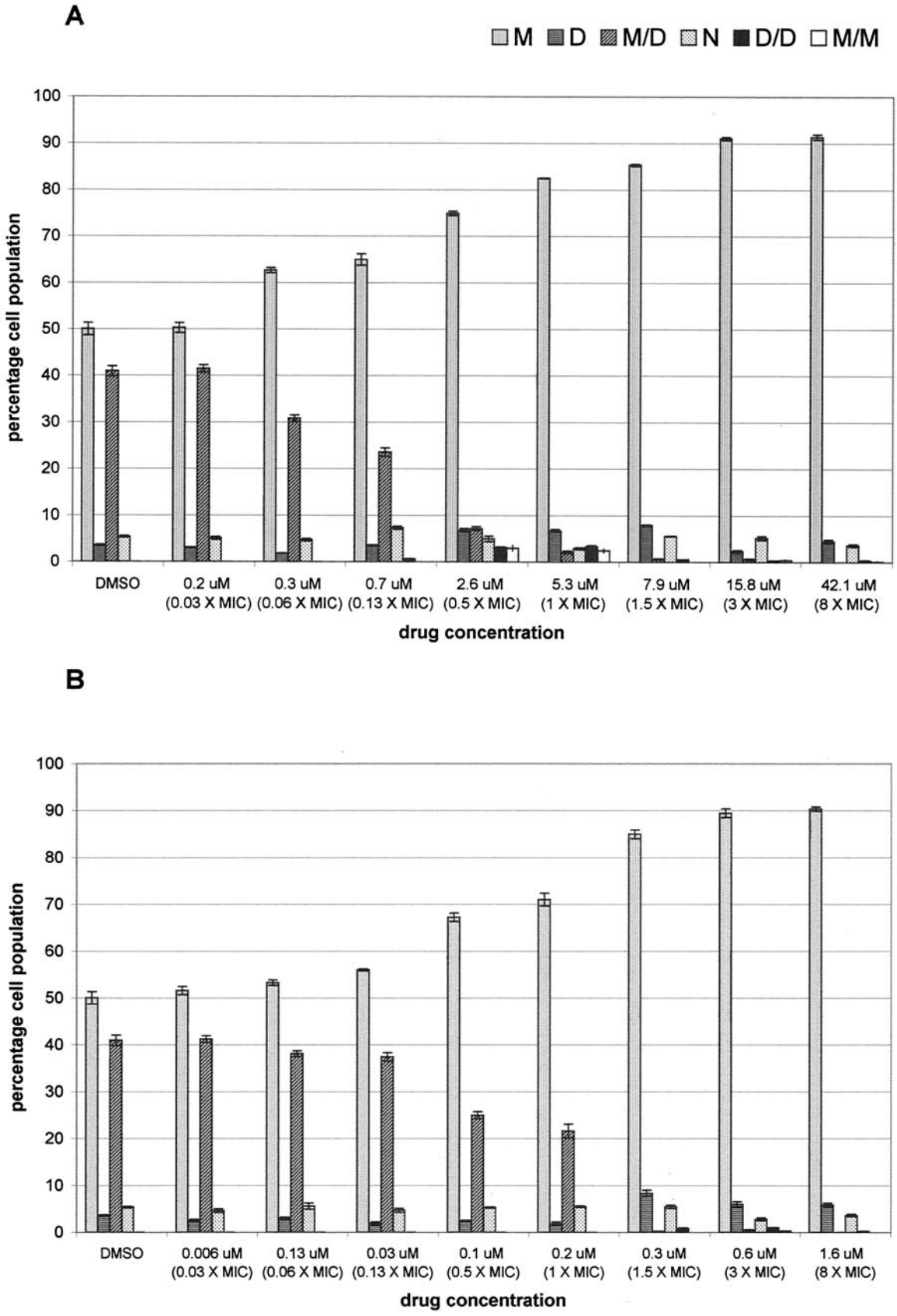

FIG. 4. Nuclear orientations of *C. neoformans* cells treated with auristatin PHE (A) or nocodazole (B). Cells were fixed 3.5 h after treatment with DMSO alone for controls or with 0.03 to 8 times the MIC of either drug (0.2 to 42.1 μM auristatin PHE; 0.006 to 1.6 μM nocodazole). Nuclei were either in the mother cell (M), in the daughter cell (D), in both (M/D), or in the neck (N), or two nuclei were present in the bud (D/D) or in the mother cell (M/M). Bars, means ± standard errors of the means for three independent experiments.

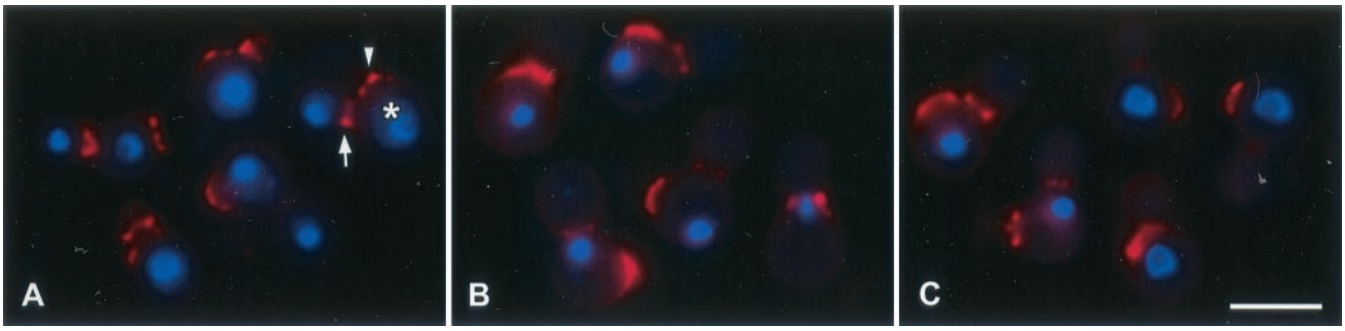

FIG. 5. Standard fluorescent imaging of inhibition of nuclear migration and division in drug-treated *C. neoformans* cells. Chitin staining using wheat-germ agglutinin conjugated with TRITC revealed chitin rings at the bud neck (arrow) and bud scars (arrowhead) on previously divided mother cells (asterisk). The TRITC label was merged with DAPI labeling. Cells were fixed 3.5 h after treatment with either DMSO alone (control) (A), 7.9 μM auristatin PHE (1.5 times the MIC) (B), or 0.3 μM nocodazole (1.5 times the MIC) (C). Bar, 5 μm.

DISCUSSION

Organization of the microtubule cytoskeleton and drug-induced disruption. In mammalian cells, the sea hare-derived peptide dolastatin 10 and its synthetic derivative auristatin PHE inhibit in vitro tubulin polymerization and the binding of vinblastine and GTP to mammalian tubulin (36, 37). In the fungus *Uromyces appendiculatus*, dolastatin 10 disrupts microtubules (41). We recently reported that a 4-h exposure to ≥2.6 μM auristatin PHE (4 times the MIC, as determined in RPMI medium) resulted in a *C. neoformans* population consisting almost entirely (~97%) of large-budded cells (50). These results led us to evaluate the effects of auristatin PHE on the microtubule organization of *C. neoformans* and to compare them to those of a compound known to interfere with the microtubule cytoskeleton in yeast (17, 21). Protocols for visualizing the microtubule network of *C. neoformans* were optimized by using immunofluorescence methods described for yeasts (40), and conditions resulting in the most consistent and thorough microtubule labeling were defined. In addition, we found that iterative deconvolution microscopy yielded much greater detail than standard two-dimensional epifluorescence microscopy or confocal microscopy. To our knowledge, the microtubule network of *C. neoformans* had not been described by use of immunofluorescence until last year (23). In the previous study (23), formaldehyde-fixed cells were made permeable with lysing enzymes from *Trichoderma harzianum*, and stained cells were examined by standard epifluorescence microscopy. These authors also noted distinct arrangements of the cryptococcal microtubule cytoskeleton during the vegetative cell cycle and found microtubule topology and dynamics to be similar to those of the fission yeast *Schizosaccharomyces*. Our results suggest that the microtubule topology of *C. neoformans* is unique within the fungi due to the presence not only of longitudinal microtubule arrangements but also of abundant tangential microtubule arrangements.

Application of our optimized labeling protocol in conjunction with deconvolution technology enabled detailed visualization of the effects of the anticryptococcal peptide auristatin PHE and the broad-spectrum benzimidazole nocodazole. Nocodazole binds β-tubulin and interferes with microtubule assembly in both animal and fungal cells in vitro and in vivo (8, 10, 14, 17, 21, 24, 34, 44). Auristatin PHE and nocodazole caused complete disruption of both spindle and cytoplasmic microtubules in *C. neoformans*. In the presence of either drug, spindle microtubules were more stable than cytoplasmic microtubules, which disappeared first. Jacobs et al. (17) also observed this phenomenon in nocodazole-treated *S. cerevisiae* via immunofluorescent tubulin staining and electron microscopy. The patterns of disruption caused by the two compounds differed in the concentration required and the rate. At the MIC, it took 4.5 h for nocodazole to cause a visible antimicrotubule effect, whereas *C. neoformans* exposed to 0.5 times the auristatin PHE MIC exhibited a completely disrupted microtubule cytoskeleton after 4.5 h. However, once the process started, nocodazole led to a more rapid microtubule disruption. To our knowledge, this is the first description of the effect of nocodazole on cryptococcal microtubules at the immunofluorescence level.

In nocodazole-treated *Saccharomyces*, disassembled microtubules have been reported to remain at or near the spindle pole bodies (SPBs) visualized as tubulin plaques, which are normally located close together (13, 16, 17). The loss of microtubules in *S. cerevisiae* does not interfere with SPB duplication but blocks SPB separation (17). In contrast, tubulin plaques in budding-arrested *C. neoformans* treated with auristatin PHE or nocodazole were not located in close proximity but instead were in the mother cell and daughter cell. Whether these remain at or near the SPBs in *C. neoformans* is not known.

Blockage of nuclear migration and mitosis, and cell cycle arrest. Intranuclear as well as cytoplasmic microtubules are crucial for nuclear elongation and division in budding yeasts (16, 17, 22), fission yeasts (47, 48), *Aspergillus* spp. (34), and plants (30). Auristatin PHE and nocodazole caused complete inhibition of nuclear migration and nuclear and cellular division in *C. neoformans*, which is likely a consequence of the microtubule disruption caused by the compounds. Models of nuclear migration in *S. cerevisiae* suggest that cytoplasmic microtubules interact with a cell component (asymmetrically distributed) which through the SPB applies a force to the nucleus and spindle (4) and that the migration of the nucleus to the neck is mediated by the capture of microtubule ends at one

cortical region at the incipient bud site, followed by microtubule depolymerization (1). Such models for nuclear migration into the daughter cell do not exist for *C. neoformans* to date. As in other basidiomycetous yeasts, mitosis occurs within the daughter cell in *C. neoformans* (26, 27, 45), and this has been described in detail by use of electron microscopy (31, 32). Quantitation of nuclear locations in auristatin PHE- or nocodazole-treated *C. neoformans* revealed a concentration-dependent increase in uninucleate cells, with the nucleus located in the mother cell, while binucleate arrangements decreased. Our results suggest that cells that had undergone mitosis at the point of drug treatment finished the cell cycle in progress. We presume that in the following drug-exposed cell cycle, cells proceeded until they reached nuclear migration, where they arrested, leading to the accumulation of uninucleate, large-budded cells (with the nucleus located randomly within the mother cell). A phenomenon seen only in auristatin PHE-treated cells was a small percentage of binucleate cells with both nuclei located in the mother cell. Interestingly, this arrangement was seen only at intermediate concentrations of auristatin PHE. This aberrant arrangement could be the result of mitosis occurring in the bud with both nuclei translocated back to the mother, or it could result from mitosis occurring in the mother cell.

Conclusions about mechanisms of action. Yeast tubulins diverged from the animal tubulins approximately 1,100 million years ago and are, in general, more homologous to animal tubulins than to tubulins from other eukaryotic organisms (9). In *C. neoformans*, there are two β-tubulin genes, *TUB1* and *TUB2. TUB1* is more conserved and more highly expressed and encodes a β-tubulin with approximately 81, 82, and 84% homology to β-tubulins from *Aspergillus nidulans*, humans, and *Schizophyllum commune*, respectively (7). Benzimidazoles such as nocodazole have been shown to specifically interact with the β-tubulin subunit of fungal microtubules (12, 19, 25, 35, 46). In *C. neoformans*, TUB1 β-tubulin is believed to represent the primary benzimidazole target (7), and it may also be the target of auristatin PHE. Auristatin PHE has been shown to inhibit the in vitro polymerization of mammalian tubulin (37). Our microscopic observations with *C. neoformans* suggest that auristatin PHE may have the same effect in this yeast; however, spectrophotometrical results with purified cryptococcal tubulin will be required to distinguish inhibition of polymerization from drug-induced depolymerization. A genetic approach to identify *C. neoformans* targets by using auristatin PHE-resistant mutants, as well as other nonlethal mutants, is under way. While nocodazole and auristatin PHE are remarkably different in structure and spectrum of activity, they appear, on the ultrastructural level at least, to have similar modes of action.

ACKNOWLEDGMENTS

This research was supported by the Arizona Disease Control Research Commission; Outstanding Investigator awards CA44344-08-12 and CA90441-01 (to G.R.P.) from the Division of Cancer Treatment and Diagnosis, NCI, DHHS; and the Robert B. Dalton Endowment.

We thank Dennis P. McDaniel for assistance with microscopy and image analysis. Light microscopy was performed in the W. M. Keck Bioimaging Laboratory (ASU).

REFERENCES

1. **Adames, N. R., and J. A. Cooper.** 2000. Microtubule interactions with the cell cortex causing nuclear movements in *Saccharomyces cerevisiae*. J. Cell Biol. **149:**863–874.
2. **Agard, D. A., Y. Hiraoka, P. Shaw, and J. W. Sedat.** 1989. Fluorescence microscopy in three dimensions. Methods Cell Biol. **30:**353–377.
3. **Amberg, D. C.** 1998. Three-dimensional imaging of the yeast actin cytoskeleton through the budding cell cycle. Mol. Biol. Cell **9:**3259–3262.
4. **Botstein, D., D. Amberg, J. Mulholland, T. Huffaker, A. Adams, D. Drubin, and T. Stearns.** 1997. The yeast cytoskeleton, p. 1–90. *In* J. R. Pringle, J. R. Broach, and E. W. Jones (ed.), The molecular and cellular biology of the yeast *Saccharomyces*. Cell cycle and cell biology. Cold Spring Harbor Laboratory Press, Cold Spring Harbor, N.Y.
5. **Busse, O.** 1894. Ueber parasitaere Zelleinschluesse und ihre Zuechtung. Zentbl. Bakteriol. **16:**175–180.
6. **Casadevall, A., and J. R. Perfect.** 1998. *Cryptococcus neoformans*. ASM Press, Washington, D.C.
7. **Cruz, M. C., and T. Edlind.** 1997. β-Tubulin genes and the basis for benzimidazole sensitivity of the opportunistic fungus *Cryptococcus neoformans*. Microbiology **143:**2003–2008.
8. **Davidse, L. C., and W. Flach.** 1977. Differential binding of methyl benzimidazol-2-yl carbamate to fungal tubulin as a mechanism of resistance to this antimitotic agent in mutant strains of *Aspergillus nidulans*. J. Cell Biol. **72:**174–193.
9. **Dayhoff, M. O.** 1978. Atlas of protein sequence and structure, vol. 5, suppl. 3. National Biomedical Research Foundation, Washington, D.C.
10. **De Brabander, M. J., R. M. Van de Veire, F. E. Aerts, M. Borgers, and P. A. Janssen.** 1976. The effects of methyl(5-(2-thienylcarbonyl)-1H-benzimidazol-2-yl) carbamate, (R 17934; NSC 238159), a new synthetic antitumoral drug interfering with microtubules, on mammalian cells cultured in vitro. Cancer Res. **36:**905–916.
11. **de Gans, J., P. Portegies, G. Tiessens, J. K. Eeftinck Schattenkerk, C. J. van Boxtel, R. J. van Ketel, and J. Stam.** 1992. Itraconazole compared with amphotericin B plus flucytosine in AIDS patients with cryptococcal meningitis. AIDS **6:**185–190.
12. **Fujimura, M., K. Oeda, H. Inoue, and T. Kato.** 1992. A single amino-acid substitution in the beta-tubulin gene of *Neurospora* confers both carbendazim resistance and diethofencarb sensitivity. Curr. Genet. **21:**399–404.
13. **Hasek, J., J. Svobodova, and E. Streiblova.** 1986. Immunofluorescence of the microtubular skeleton in growing and drug-treated yeast protoplasts. Eur. J. Cell Biol. **41:**150–156.
14. **Hoebeke, J., G. Van Nijen, and M. De Brabander.** 1976. Interaction of oncodazole (R 17934), a new antitumoral drug, with rat brain tubulin. Biochem. Biophys. Res. Commun. **69:**319–324.
15. **Hogan, L. H., B. S. Klein, and S. M. Levitz.** 1996. Virulence factors of medically important fungi. Clin. Microbiol. Rev. **9:**469–488.
16. **Huffaker, T. C., J. H. Thomas, and D. Botstein.** 1988. Diverse effects of beta-tubulin mutations on microtubule formation and function. J. Cell Biol. **106:**1997–2010.
17. **Jacobs, C. W., A. E. Adams, P. J. Szaniszlo, and J. R. Pringle.** 1988. Functions of microtubules in the *Saccharomyces cerevisiae* cell cycle. J. Cell Biol. **107:**1409–1426.
18. **Joseph-Horne, T., D. Hollomon, R. S. Loeffler, and S. L. Kelly.** 1995. Cross-resistance to polyene and azole drugs in *Cryptococcus neoformans*. Antimicrob. Agents Chemother. **39:**1526–1529.
19. **Jung, M. K., I. B. Wilder, and B. R. Oakley.** 1992. Amino acid alterations in the *benA* (beta-tubulin) gene of *Aspergillus nidulans* that confer benomyl resistance. Cell Motil. Cytoskeleton **22:**170–174.
20. **Kelly, S. L., D. C. Lamb, M. Taylor, A. J. Corran, B. C. Baldwin, and W. G. Powderly.** 1994. Resistance to amphotericin B associated with defective sterol δ 8→7 isomerase in a *Cryptococcus neoformans* strain from an AIDS patient. FEMS Microbiol. Lett. **122:**39–42.
21. **Kilmartin, J. V.** 1981. Purification of yeast tubulin by self-assembly in vitro. Biochemistry **20:**3629–3633.
22. **King, S. M., and J. S. Hyams.** 1982. The mitotic spindle of *Saccharomyces cerevisiae*: assembly, structure and function. Micron **13:**93–117.
23. **Kopecka, M., M. Gabriel, K. Takeo, M. Yamaguchi, A. Svoboda, M. Ohkusu, K. Hata, and S. Yoshida.** 2001. Microtubules and actin cytoskeleton in *Cryptococcus neoformans* compared with ascomycetous budding and fission yeasts. Eur. J. Cell Biol. **80:**303–311.
24. **Lee, J. C., D. J. Field, and L. L. Lee.** 1980. Effects of nocodazole on structures of calf brain tubulin. Biochemistry **19:**6209–6215.
25. **Li, J., S. K. Katiyar, and T. D. Edlind.** 1996. Site-directed mutagenesis of *Saccharomyces cerevisiae* beta-tubulin: interaction between residue 167 and benzimidazole compounds. FEBS Lett. **385:**7–10.
26. **McCully, E. K., and C. F. Robinow.** 1972. Mitosis in heterobasidiomycetous yeasts. I. *Leucosporidium scottii* (*Candida scottii*). J. Cell Sci. **10:**857–881.
27. **McCully, E. K., and C. F. Robinow.** 1972. Mitosis in heterobasidiomycetous yeasts. II. *Rhodosporidium* sp. (*Rhodotorula glutinis*) and *Aessosporon salmonicolor* (*Sporobolomyces salmonicolor*). J. Cell Sci. **11:**1–31.
28. **McNally, J. G., T. Karpova, J. Cooper, and J. A. Conchello.** July 1999.

Three-dimensional imaging by deconvolution microscopy. Methods **19:**373–385.
29. **Meunier, F.** 1991. Fungal infections in cancer patients. Cancer Investig. **9:**151–158.
30. **Mineyuki, Y., and M. Furuya.** 1985. Involvement of microtubules on nuclear positioning during apical growth in *Adiantum protonemata*. Plant Cell Physiol. **26:**627–634.
31. **Mochizuki, T.** 1998. Three-dimensional reconstruction of mitotic cells of *Cryptococcus neoformans* based on serial section electron microscopy. Nippon Ishinkin Gakkai Zasshi **39:**123–127. (In Japanese.)
32. **Mochizuki, T., S. Tanaka, and S. Watanabe.** 1987. Ultrastructure of the mitotic apparatus in *Cryptococcus neoformans*. J. Med. Vet. Mycol. **25:**223–233.
33. **National Committee for Clinical Laboratory Standards.** 1997. Reference method for broth dilution antifungal susceptibility testing of yeasts: approved standard M27-A. National Committee for Clinical Laboratory Standards, Wayne, Pa.
34. **Oakley, B. R., and N. R. Morris.** 1981. A beta-tubulin mutation in *Aspergillus nidulans* that blocks microtubule function without blocking assembly. Cell **24:**837–845.
35. **Orbach, M. J., E. B. Porro, and C. Yanofsky.** 1986. Cloning and characterization of the gene for beta-tubulin from a benomyl-resistant mutant of *Neurospora crassa* and its use as a dominant selectable marker. Mol. Cell. Biol. **6:**2452–2461.
36. **Pettit, G. R.** 1997. The dolastatins. Fortschr. Chem. Org. Naturst. **70:**1–79.
37. **Pettit, G. R., J. K. Srirangam, J. Barkoczy, M. D. Williams, M. R. Boyd, E. Hamel, R. K. Pettit, F. Hogan, R. Bai, J. C. Chapuis, S. C. McAllister, and J. M. Schmidt.** 1998. Antineoplastic agents 365. Dolastatin 10 SAR probes. Anticancer Drug Des. **13:**243–277.
38. **Pettit, G. R., and J. K. Srirangam.** July 1998. U.S. patent 5,780,588.
39. **Pettit, R. K., G. R. Pettit, and K. C. Hazen.** 1998. Specific activities of dolastatin 10 and peptide derivatives against *Cryptococcus neoformans*. Antimicrob. Agents Chemother. **42:**2961–2965.
40. **Pringle, J. R., A. E. Adams, D. G. Drubin, and B. K. Haarer.** 1991. Immunofluorescence methods for yeast. Methods Enzymol. **194:**565–602.
41. **Roberson, R. W., B. Tucker, and G. R. Pettit.** 1998. Microtubule depolymerization in *Uromyces appendiculatus* by three new antineoplastic drugs: combretastatin A-4, dolastatin 10 and halichondrin B. Mycol. Res. **102:**378–382.
42. **Samonis, G., and D. Bafaloukos.** 1992. Fungal infections in cancer patients: an escalating problem. In Vivo **6:**183–193.
43. **Scalettar, B. A., J. R. Swedlow, J. W. Sedat, and D. A. Agard.** 1996. Dispersion, aberration and deconvolution in multi-wavelength fluorescence images. J. Microsc. **182:**50–60.
44. **Schulze, E., and M. Kirschner.** 1987. Dynamic and stable populations of microtubules in cells. J. Cell Biol. **104:**277–288.
45. **Taylor, J. W., and K. Wells.** 1979. A light and electron microscopic study of mitosis in *Bullera alba* and the histochemistry of some cytoplasmic substances. Protoplasma **98:**31–62.
46. **Thomas, J. H., N. F. Neff, and D. Botstein.** 1985. Isolation and characterization of mutations in the beta-tubulin gene of *Saccharomyces cerevisiae*. Genetics **111:**715–734.
47. **Toda, T., K. Umesono, A. Hirata, and M. Yanagida.** 1983. Cold-sensitive nuclear division arrest mutants of the fission yeast *Schizosaccharomyces pombe*. J. Mol. Biol. **168:**251–270.
48. **Umesono, K., T. Toda, S. Hayashi, and M. Yanagida.** 1983. Cell division cycle genes *nda2* and *nda3* of the fission yeast *Schizosaccharomyces pombe* control microtubular organization and sensitivity to anti-mitotic benzimidazole compounds. J. Mol. Biol. **168:**271–284.
49. **van der Horst, C. M., M. S. Saag, G. A. Cloud, R. J. Hamill, J. R. Graybill, J. D. Sobel, P. C. Johnson, C. U. Tuazon, T. Kerkering, B. L. Moskovitz, W. G. Powderly, W. E. Dismukes, et al.** 1997. Treatment of cryptococcal meningitis associated with the acquired immunodeficiency syndrome. N. Engl. J. Med. **337:**15–21.
50. **Woyke, T., G. R. Pettit, G. Winkelmann, and R. K. Pettit.** 2001. In vitro activities and postantifungal effects of the potent dolastatin 10 derivative auristatin PHE. Antimicrob. Agents Chemother. **45:**3580–3584.